ATR Inhibitor AZD6738 (Ceralasertib) Exerts Antitumor Activity as a Monotherapy and in Combination with Chemotherapy and the PARP Inhibitor Olaparib

Zena Wilson[1], Rajesh Odedra[1], Yann Wallez[2], Paul W.G. Wijnhoven[2], Adina M. Hughes[1], Joe Gerrard[3], Gemma N. Jones[3], Hannah Bargh-Dawson[3], Elaine Brown[1], Lucy A. Young[2], Mark J. O'Connor[2], and Alan Lau[2]

ABSTRACT

AZD6738 (ceralasertib) is a potent and selective orally bioavailable inhibitor of ataxia telangiectasia and Rad3-related (ATR) kinase. ATR is activated in response to stalled DNA replication forks to promote G_2–M cell-cycle checkpoints and fork restart. Here, we found AZD6738 modulated CHK1 phosphorylation and induced ATM-dependent signaling (pRAD50) and the DNA damage marker γH2AX. AZD6738 inhibited break-induced replication and homologous recombination repair. *In vitro* sensitivity to AZD6738 was elevated in, but not exclusive to, cells with defects in the ATM pathway or that harbor putative drivers of replication stress such as CCNE1 amplification. This translated to *in vivo* antitumor activity, with tumor control requiring continuous dosing and free plasma exposures, which correlated with induction of pCHK1, pRAD50, and γH2AX. AZD6738 showed combinatorial efficacy with agents associated with replication fork stalling and collapse such as carboplatin and irinotecan and the PARP inhibitor olaparib. These combinations required optimization of dose and schedules *in vivo* and showed superior antitumor activity at lower doses compared with that required for monotherapy. Tumor regressions required at least 2 days of daily dosing of AZD6738 concurrent with carboplatin, while twice daily dosing was required following irinotecan. In a BRCA2-mutant patient-derived triple-negative breast cancer (TNBC) xenograft model, complete tumor regression was achieved with 3 to5 days of daily AZD6738 per week concurrent with olaparib. Increasing olaparib dosage or AZD6738 dosing to twice daily allowed complete tumor regression even in a *BRCA* wild-type TNBC xenograft model. These preclinical data provide rationale for clinical evaluation of AZD6738 as a monotherapy or combinatorial agent.

Significance: This detailed preclinical investigation, including pharmacokinetics/pharmacodynamics and dose–schedule optimizations, of AZD6738/ceralasertib alone and in combination with chemotherapy or PARP inhibitors can inform ongoing clinical efforts to treat cancer with ATR inhibitors.

Introduction

Ataxia telangiectasia and Rad3-related (ATR) is a serine/threonine protein kinase involved in coordinating cell-cycle checkpoints and DNA damage response (DDR) caused by DNA replication–associated stress (1, 2). Replication stress is defined as the stalling of DNA replication fork progression, and persistent replication stress leads to genomic instability and lethality if unrepaired. ATR is recruited and activated by regions of single-strand DNA coated with replication protein A (RPA) that are created upon replication fork stalling or during DNA end resection during double-strand break (DSB) repair. ATR activation leads to slowing fork progression and stabilization to prevent its collapse and formation of single-ended DSBs. ATR also initiates G_2–M cell-cycle arrest through phosphorylation/activation of CHK1 kinase, which provides time to complete repair and prevent cells from entering mitosis with damaged DNA.

Targeting ATR has shown promising antitumor activity in preclinical models and multiple ATR inhibitors (ATRi) are in phase I/II clinical development as anticancer agents (3–5). AZD6738 (ceralasertib) is an oral and selective inhibitor of ATR (6) in clinical development as monotherapy or in combination with chemotherapy, IR, PARP inhibitors or immunotherapy agents. Preclinical studies have suggested enhanced sensitivity to ATRi in models with DSB repair defects in particular ATM-loss (7–14), oncogene activation (3), and genomic instability drivers such as through APOBECs (15, 16), PBGD5-transposase (17), SWI-SNF (18, 19), or defective transcriptional processing (20, 21). ATR's role in response to replication stress also suggests ATRis should mechanistically combine well with replication-associated DNA-damaging agents to potentiate their antitumor activity. Several preclinical studies support this notion and ATRis show combination activity with IR (22–24) and chemotherapy agents such cisplatin (25), irinotecan (26), bendamustine (27), and gemcitabine (28) as well as PARP inhibitors (29, 30).

The rationale of ATR kinase inhibitors is to target cancers susceptible to high replication stress and promoting lethality either as monotherapy or in combination. Identifying cancers sensitive to ATR inhibition and optimizing dose schedules are key to their clinical

[1]Bioscience, Oncology R&D, AstraZeneca, Cheshire, United Kingdom. [2]Bioscience, Oncology R&D, AstraZeneca, Cambridge, United Kingdom. [3]Translational Medicine, Oncology R&D, AstraZeneca, Cambridge, United Kingdom.

Note: Supplementary data for this article are available at Cancer Research Online (http://cancerres.aacrjournals.org/).

Current address for R. Odedra: Evotec (UK) Ltd, Cheshire, United Kingdom; and current address for H. Bargh-Dawson, The Institute of Cancer Research, London, United Kingdom.

Corresponding Author: Alan Lau, Bioscience, Oncology R&D, AstraZeneca, Hodgkin Building, C/O Darwin Building, Unit 310, Cambridge Science Park, Milton Road, Cambridge CB4 OWG, United Kingdom. Phone: 4407-9171-88399; E-mail: alan.lau@astrazeneca.com

Cancer Res 2022;82:1140–52

doi: 10.1158/0008-5472.CAN-21-2997

success. Here we describe the preclinical activity of the orally bioavailable ATR kinase inhibitor AZD6738 as monotherapy and optimization of dose-schedules in combination agents that cause replication stress.

Materials and Methods

Cell line culture and compounds

All cell lines were cultured at 37°C, 5% CO_2, and authenticated DNA fingerprinting short tandem repeat assay. All cells lines passed *Mycoplasma* and mouse IMPACT tests. The genomics of the cell lines was acquired from public databases CCLE and COSMIC. AZD6738 and olaparib were made by AstraZeneca.

Cell panel growth inhibition assays

Cells were seeded in 96-well plates at a density to allow for logarithmic growth during treatment. Cells were treated for 3 days and cell proliferation measured by MTS CellTiter Proliferation Assay (Promega). The concentration where growth is inhibited 50% versus untreated cells (GI_{50}) were determined. Unpaired Mann–Whitney *t* test was used to determine statistical differences [GraphPad Prism; nonsignificant (ns), $P > 0.05$; *, $P \le 0.05$; **, $P \le 0.01$; ***, $P \le 0.001$; ****, $P \le 0.0001$].

In vitro combinations and synergy scores

Cancer cell line panel screening has been previously described (31). Combination synergy scores for each combination were calculated based on the Loewe model of additivity. Synergy scores of ∼0 are indicative of additive effect. Higher synergy scores (>1) indicate greater enhancement of activity more than expected as monotherapy with scores 1 to 5 showing overall net antiproliferative or weak synergistic effect, while scores above a >5 having overall net cell killing effect or strong synergy.

Break-induced replication and traffic light reporter assays

A549 cells stably expressing a break-induced replication (BIR) reporter construct (32) or HEK293 cells expressing the traffic light reporter (TLR) reporter (33), both harboring a Cas9 recognition site, were transiently transfected with a mammalian expression plasmid containing *Cas9* and a BIR or TLR-reporter allele-directing guide-RNA. To induce homologous recombination repair (HRR) cells were electroporated with a plasmid containing a GFP donor template. Cells were treated for 24 (HEK293-TLR) or 72 (A549-BIR) hours. Detection of GFP-positive cells representing the HRR-positive populations or mCherry-positive cells (TLR) through mutagenic end joining-mediated DSB repair were performed by flow cytometry (BD FACSAria). %GFP-positive cells representing BIR or gene conversion (TLR) were calculated (FlowJo) and normalized to the combined $S–G_2$ populations of the vehicle control to account for impact of treatment on cell-cycle distributions. Statistical significance was evaluated using an unpaired Mann–Whitney *t* test (GraphPad Prism, as above).

Metaphase spread analysis

BRCA1Δ11q mutant or BRCA1 complemented UWB1.289 ovarian cancer cells (34) were seeded into 10-cm dishes. Cells were treated for 72 hours. 67 hours posttreatment, cells were incubated with 30 ng/mL Colcemid (KaryoMAX Colcemid ThermoFisher) for further 5 hours. Cells were detached then resuspended in hypotonic solution (0.075 M KCl) and incubated at 37°C for 12 minutes. Cells were fixed with 3 cycles of ice-cold fixative (3:1, methanol:acetic acid; Sigma-Aldrich). Pellets were washed a further 3x then cell suspensions dropped onto microscope slides (Superfrost Plus and ColorFrost Plus; VWR) and stained with 8% Giesma (Sigma-Aldrich). Cover slips were mounted onto microscope slides using DPX Mountant (Sigma-Aldrich). Chromosomal aberrations described as chromatid or chromosome breaks and fusions were scored by eye for 25–50 metaphase spreads per sample using the Metafer 4 system (Metasystems).

In vivo studies

Animal studies were approved and performed in accordance with local regulations (Home Office, UK), the Animal Scientific Procedures Act 1986, guidelines established by the internal Institutional Animal Care and Use Committee and the AstraZeneca Global Bioethics policy. Data were reported following the ARRIVE guidelines (35). *In vivo* tolerability/body weight loss (BWL) and welfare checks were conducted in 6 to 9 week-old female athymic nude mice ($n = 3$/group) at the dose and schedules indicated. BWL ≥20% relative to the start of dosing were classified as not tolerated. Tumor xenografts were established female athymic nude mice by subcutaneous injection. Animals were randomized into treatment groups when tumors became palpable. Tumor volume (TV) was evaluated with a caliper using the formula TV (mm^3) = [length (mm) × width $(mm)^2$]/2. %Tumor growth inhibition (%TGI) was assessed by comparison of the mean change in TV for the control versus treated groups. Statistical significance was evaluated using a one-tailed *t* test (ns, $P > 0.05$; *, $P \le 0.05$; **, $P \le 0.01$; ***, $P \le 0.001$).

AZD6738 was formulated in 10% DMSO/40% Propylene Glycol (Sigma-Aldrich)/50% deionized water and dosed at 0.1 mL/10 g orally. Carboplatin was administered by intraperitoneal injection at 30 mg/kg once daily every two weeks. Irinotecan was administered by intraperitoneal injection at 20 mg/kg once daily every two weeks. Olaparib was dosed orally at the dose/schedules indicated.

Patient-derived tumor explant models

Human patient-derived tumor explant (PDX) models were previously established in immunodeficient mice and studies conducted by Xentech, and previously molecularly and functionally characterized for PARP inhibitor activity and BRCA/HRR status (36). HBCx-9 is a triple-negative breast cancer (TNBC) ductal adenocarcinoma with mutated TP53 (V143 fs25aaTer), ATM (Q1128R) and CDH1 (A617T) but wild-type (WT) for BRCA1/2, RB1, and PTEN. HBCx-9 is high for Rad51 foci and considered HR-proficient. The ATM mutation is not considered deleterious and HBCx-9 has intact ATM signaling and function (37). HBCx-10 is a TNBC ductal adenocarcinoma with mutated BRCA2 (Q2036*) and TP53 (V157F), with RB1 and PTEN deleted. HBCx-10 is low for Rad51 foci and considered HR-deficient.

In vivo pharmacokinetics, Western blots, and pharmacodynamics

For blood plasma pharmacokinetic analysis, Western blots, and IHC staining and quantification for γH2AX, CHK1 pSer345, and Rad50 pSer635 on tumor samples were performed as previously described (6, 7, 38).

Data were generated by the authors and included in the article or available on request.

Results

AZD6738 selectively inhibits specific cell lines *in vitro*

AZD6738 (**Fig. 1A**) is a sulfoximine morpholino-pyrimidine ATRi that is currently in phase I/II clinical trials. It is a highly selective, ATP-competitive inhibitor that is orally bioavailable with high

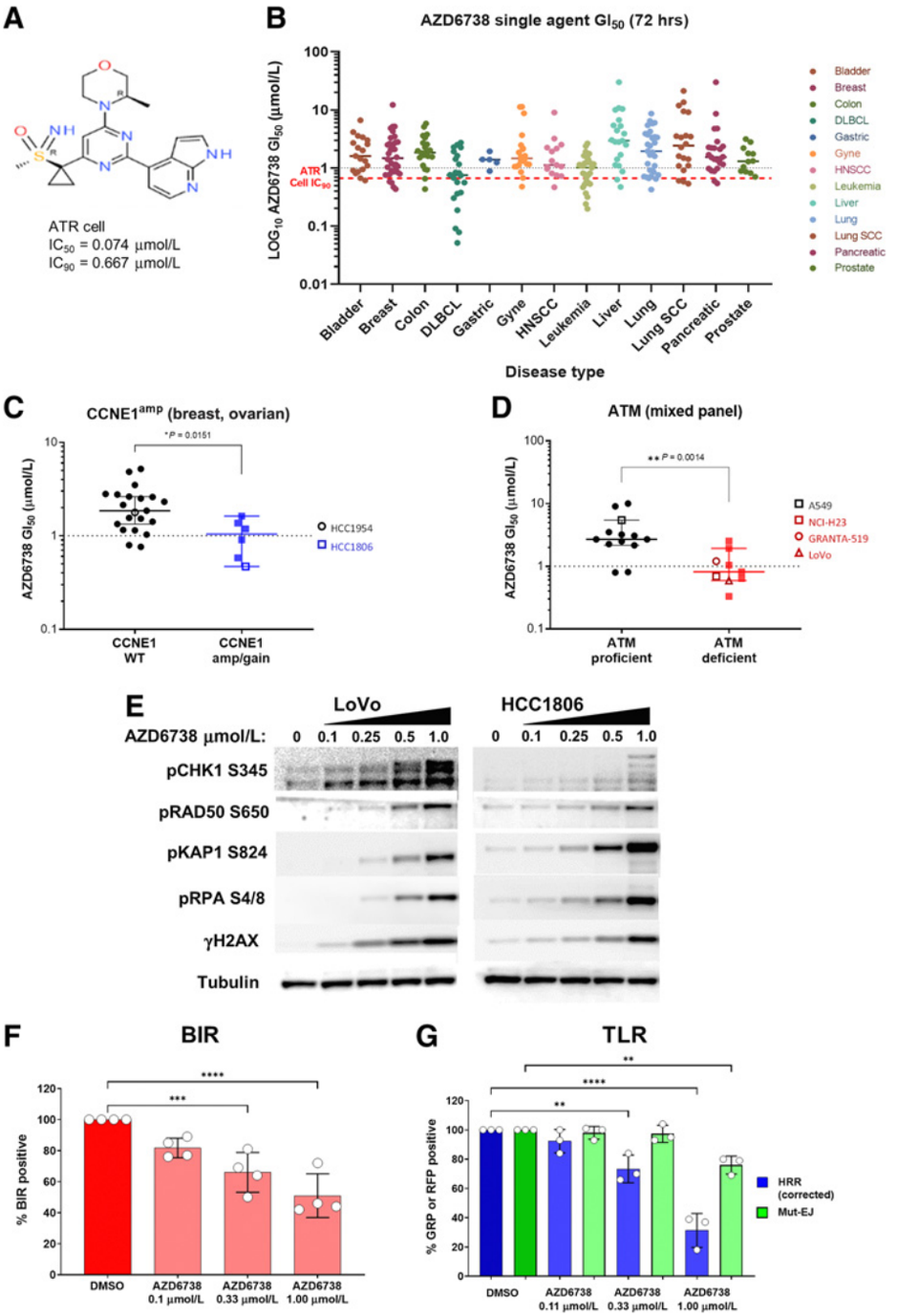

Figure 1.

In vitro activity of AZD6738 (ceralasertib). **A,** Chemical structure of AZD6738. **B,** Scatter plots of the GI_{50} values for all cell lines. Selected cell lines grouped by **C** and **D,** CCNE1 amplification (**C**) or ATM signaling status classification (**D**). Each cell line is labeled by a dot and the median $GI_{50} \pm 95\%$ CI. **E,** Western blot of CHK1 pSer345, ATM signaling (RAD50 pSer635, KAP1 pSer824), replication stress (RPA pSer4/8), and γH2AX 24 hours after AZD6738 treatment at the indicated concentrations of AZD6738 in LoVo ($MRE11A^{del}$) and HCC1806 ($CCNE1^{amp}$) cell line. **F,** AZD6738 inhibition of BIR in A549-BIR assay reporter cells. **G,** AZD6738 inhibition of HRR but not mutagenic end-joining (mut-EJ) repair in 293T-TLR assay reporter cells. **, $P \leq 0.01$; ***, $P \leq 0.001$; ****, $P \leq 0.0001$.

aqueous solubility and no CYP3A4 time-dependent inhibition. While AZD6738 chemical synthesis, kinase selectivity and basic biochemical properties have been described (6), here we sought to expand these findings by more comprehensively characterizing the cellular activity and biological consequences of AZD6738 treatment.

To investigate the *in vitro* activity, we identified cancer cell lines that showed sensitivity to single agent AZD6738, within the "on-target" concentration ranges (IC_{50-90} = 0.074–0.67 µmol/L; ref. 6). Growth-inhibitory activity of AZD6738 was assessed across 276 different cancer cell lines representing different histologies (**Fig. 1B**). The median 50% growth inhibition GI_{50} (1.47 µmol/L) was above ATR cell IC_{90} for most cell lines and only 13% of cell lines ($n = 38$) had GI_{50} less than median and 30% below 1 µmol/L. Hematologic cell lines (median GI_{50} = 0.82 µmol/L) showed generally enhanced sensitivity compared with solid tumor cells (median GI_{50} = 1.68 µmol/L).

When comparing "sensitive" (<1 µmol/L) versus "in-sensitive" cell lines a single unifying molecular aberration could not be identified explaining sensitivity, although mutations in specific diseases did show statistically significant enrichments. Within this dataset we found associations with *CCNE1* gain/amplifications in breast and ovarian

cell lines (**Fig. 1C**), presumably due to oncogene-induced replication stress (3). We also observed significant associations with deleterious (frameshifts/stop) mutations in ARID1A, ATRX, and SETD2. We did not observe significant associations between TP53, BRCA1/2, CCND1, KRAS, or ATM mutations (Supplementary Fig. S2). The lack of an association with ATM mutations was surprising as ATM-loss has been linked to enhanced ATRi responses (4). We therefore assessed whether these cell lines showed loss of ATM functionality. We defined ATMs status through a functionality-based assessment by ability to induce ATM pSer1981 (pATM) and CHK2 pThr68 (pCHK2) 30 minutes after 6 Gy IR. Cell lines with low total ATM expression and that were unable to induce pATM and pCHK2 were classed as ATM-deficient, while cell lines that did show induction were classed as ATM-proficient (Supplementary Fig. S1). By stratifying cell lines by ATM function, we now observed a significant association with AZD6738 sensitivity (**Fig. 1D**). These data suggest that complete absence of ATM function may be required for sensitivity to ATRi.

AZD6738 activates the ATM-dependent signaling pathway and suppresses recombination-mediated DNA repair

Having identified sensitive cell lines, we further investigated the consequences of ATR inhibition on DDR pathway signaling and compensation. We treated LoVo (MRE11A-mutant) colorectal and HCC1806 ($CCNE1^{amp}$) breast cancer cells with increasing concentrations of AZD6738 for 24 hours and assessed DDR signaling by Western blot (**Fig. 1E**). We observed concentration-dependent modulation of ATR and ATM-dependent signaling pathways as well as markers of DSBs. 24-hour treatment increased CHK1 pSer345 (pCHK1) and replication-associated DSB marker RPA pSer4/8 (pRPA) with strong induction above 0.5 μmol/L. AZD6738 also induced robust phosphorylation of ATM-dependent substrates RAD50 pSer635 (pRAD50) and KAP1 pSer824 (pKAP1) as well as the DSB marker γH2AX. The induction of these markers are likely a common "on-target" consequence of ATR inhibition (as monotherapy) and not just AZD6738 as we observed similar activity with a different ATRi BAY-1895344 (Supplementary Fig. S3B). In isogenic paired ATM WT and ATM knockout FaDu cell lines, we observe induction of ATM-dependent pathway signaling in the WT cells, but in ATM knockout cells this is reversed with expression levels of both pCHK1 and pKAP1 elevated at baseline and inhibited by AZD6738, suggesting a compensatory signaling by ATR in the absence of ATM (Supplementary Fig. S3C).

To specifically investigate the mechanism of action of AZD6738 on replication-associated DNA repair processes we employed the BIR reporter assay to assess impact on replication associated single-ended DSBs repair and on HRR/mutagenic end-joining using the TLR assay. Here we observed AZD6738 was able to inhibit both BIR repair (**Fig. 1F**) and HRR (**Fig. 1G**) at concentrations >0.333 μmol/L. These data indicate ATR regulates repair of broken replication forks by HR factors shared by BIR and gene conversion.

Together, these data show significant AZD6738 biological activities against DDR and repair functions are observed at concentrations closer to cellular ATR IC_{90} (Supplementary Fig. S3). Importantly these concentrations are clinically achievable with free plasma pharmacokinetics in human phase I dose escalation studies showing that cover above ATR cell IC_{90} from 80 to 320 mg AZD6738 daily dose range (39, 40).

AZD6738 *in vivo* antitumor activity in ATM-DDR defective xenograft models correlates with drug exposure and DDR signaling biomarker induction

We next assessed whether *in vitro* activity translated to *in vivo* antitumor activity and modulation of DDR signaling pharmacodynamic biomarkers in xenograft models. We used the Granta-519 mantle cell lymphoma, LoVo colorectal, NCI-H23 non–small cell lung cancer and FaDu head and neck ATM knockout cancer models and compared those to the A549 non–small cell lung cancer and FaDu WT ATM-proficient models (Supplementary Fig. S1).

LoVo and Granta-519 (**Fig. 2A**) showed dose dependent efficacy with significant %TGI at 50 mg/kg once daily, moderate activity at 25 mg/kg and no activity at 10 mg/kg. Compared with 12.5 mg/kg twice daily dosing the antitumor activity was equivalent to 50 mg/kg once daily dose. Pharmacokinetic analysis of free plasma concentrations of AZD6738 (Supplementary Table S1) at 25 mg/kg showed C_{max} = 8.8 μmol/L/time above IC_{90} ~6 hours, while 50 mg/kg C_{max} = 18 μmol/L/time above IC_{90} ~8 hours while 12.5 mg/kg twice daily has lower C_{max} but longer time over IC_{90} ~14 hours, confirming duration of cover over IC_{90} drives antitumor activity. Significant antitumor activity was also observed in NCI-H23 but not in A549 ATM-proficient model, consistent with *in vitro* data. Comparing efficacy of different dosing schedules in the FaDu ATM knockout xenograft, significant activity is observed with continuous daily dosing at 25 or 50 mg/kg once daily but weaker growth inhibition when dosing was reduced to 3-days-on/4-days-off (**Fig. 2B**).

We assessed pharmacodynamics biomarkers for ATR and DDR in tumors. AZD6738 was dosed at 10, 25, or 50 mg/kg once daily for 3 days and tumors collected on day 4 before dosing (0 hours) or at +2 hours, +8 hours, or +24 hours after dosing on day 4. Tumor samples were stained for pCHK1, pRAD50, and γH2AX by IHC and a dose-dependent increase in all three biomarkers was observed (**Fig. 2C**). While the trends were similar, differences in the magnitude of signal were seen with pRAD50 showing largest induction (12%–18%) followed by γH2AX (8%–12%) and pCHK1 (5%–8%). The timing of peak induction and duration of signal (**Fig. 2D**) were also seen with pCHK1 being inhibited at 2 hours but then increasing by 8 hours before dropping to baseline. pRAD50 peaked by 8 hours and maintained to 24 hours. γH2AX showed peak at 2 hours and also remained elevated. Comparing %TGI with pharmacodynamics and free plasma AUC (**Fig. 2E** and **F**) showed a linear positive correlation, indicating dose- pharmacokinetics-pharmacodynamics are related to efficacy.

AZD6738 *in vivo* antitumor activity and modulation of DDR biomarkers in $CCNE1^{amp}$ xenograft model

In order to assess whether the observed relationships extends beyond models with DDR defects, we tested in a HCC1806 model, which harbors CCNE1 amplification. We assessed *in vivo* xenografts for dose-dependent efficacy and included comparisons of low dose 6.25, 12.5, 25 mg/kg twice daily versus high dose 50 mg/kg once daily (**Fig. 3A**). We observed a dose-dependent increase in efficacy with 6.25 mg/kg twice daily showing weak antitumor activity but incremental improvements in growth inhibition when increased >12.5 mg/kg twice daily. Note that we were only able to dose the 25 mg/kg twice daily group for 14 days due to tolerability, while all other groups continued to full 21 days dosing. Even so, the best growth inhibition was observed using 25 mg/kg twice daily while 12.5 mg/kg twice daily and 50 mg/kg once daily similar. In comparison, the HCC1954 breast cancer xenograft model (**Fig. 3B**) showed no response to AZD6738, consistent with the insensitivity *in vitro*.

Plasma pharmacokinetics and tumor pharmacodynamics analysis were taken at the end of study (day 21) at 2 and 6 hours after the

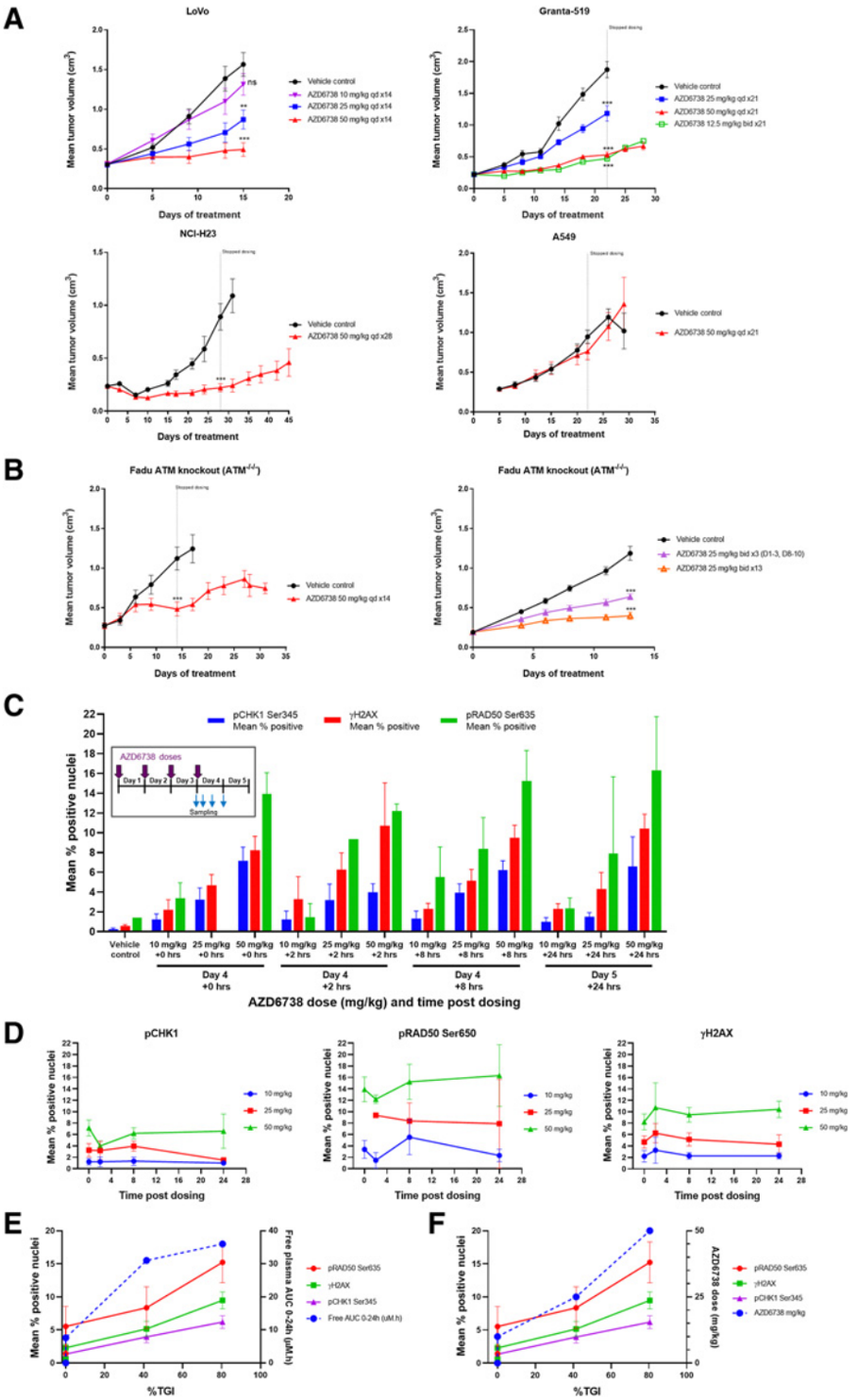

Figure 2.

Antitumor *in vivo* efficacy of AZD6738 across multiple ATM-deficient cell line xenograft models. **A** and **B,** LoVo (MRE11A), Granta-519, NCI-H23, 549 (ATM-proficient control; **A**) and FaDu ATM knockout (**B**). AZD6738 was dosed at the indicated duration and doses either once daily (qd) or twice daily (bid). Mean tumor volume ± SEM is shown. **C,** LoVo xenograft IHC pharmacodynamics for CHK1 Ser345, γH2AX, and pRAD50 Ser645 biomarkers. AZD6738 was dosed at the indicated doses once daily for 3 to 4 days and tumor harvested at time 0 (day 4, before the 4th dose) or 2, 8, or 24 hours after fourth daily dose. Mean percentage of positive staining nuclei plus SD is shown. **D,** Change in expression for each biomarker. **E,** Free plasma AUC versus %TGI for each biomarker at 8 hours. **F,** AZD6738 dose versus %TGI for each biomarker at 8 hours. ns, nonsignificant; **, $P \le 0.01$; ***, $P \le 0.001$.

last dose. Free plasma concentrations (**Fig. 3C**) for AZD6738 showed dose proportionality and 6.25 mg/kg dose drops below ATR IC_{90}/GI_{50} level by ∼5 to 6 hours, a level that was deemed to be insufficient for robust activity. Both 12.5 mg/kg twice daily and 50 mg/kg once daily groups are above this level for >6 hours. Comparing the 12.5 mg/kg twice daily and 50 mg/kg once daily C_{max} with their respective %TGI indicate that activity is not driven by high peak concentrations, as C_{max} is ∼10-fold higher at 50 mg/kg. Analysis of pRAD50 (**Fig. 3E**) also showed dose-dependent increase with AZD6738 and induction with 12.5 mg/kg twice daily being similar to 50 mg/kg once daily consistent with pharmacokinetics cover and growth inhibition activity.

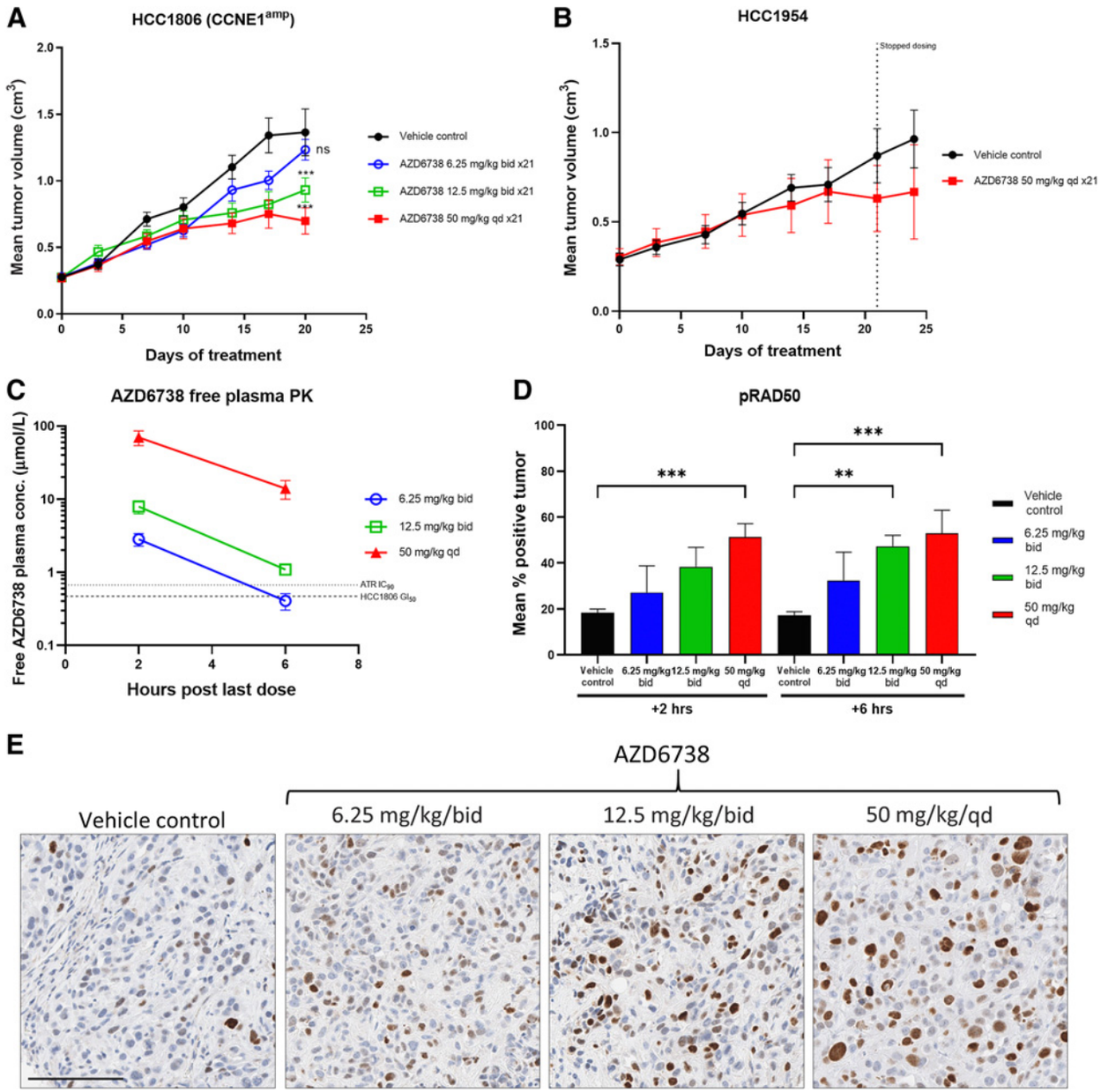

Figure 3.

Antitumor *in vivo* efficacy breast cancer cell line xenograft models. **A** and **B,** HCC1806 harboring cyclin E amplification (**A**) and WT control HCC1954 xenografts (**B**). AZD6738 was dosed at the indicated duration and doses either once daily (qd) or twice daily (bid). Mean tumor volume ± SEM are shown. End-of-efficacy (day 21) plasma pharmacokinetics (PK) and tumor pharmacodynamics were assessed for HCC1806. **C,** Free plasma AZD6738 concentration (PK) plotted against dose at 2 or 6 hours after last AZD6738 dose. **D,** Pharmacodynamics IHC quantification of percentage of tumor cells positive for pRAD50 Ser635 at 2 or 6 hours post last AZD6738 or vehicle dose. Mean percentage of positive staining nuclei plus SD is shown. **E,** Representative images of the IHC pRAD50 expression 2 hours post last dose. ns, nonsignificant; **, $P \le 0.01$; ***, $P \le 0.001$.

AZD6738 combines synergistically with platinum and antimetabolite class of chemotherapy agents *in vitro*

Mechanistically, ATRi should synergize with DNA-damaging agents, which cause replication stress. To assess the ability of AZD6738 to potentiate the cytotoxic effects of such agents, we tested combinations with chemotherapies across a panel of cell lines *in vitro*. Here, AZD6738 was added concurrently with platinum DNA-interstrand crosslinkers cisplatin, carboplatin, and oxaliplatin, Top1 inhibitors SN38 (irinotecan) and topotecan, antimetabolites gemcitabine and pemetrexed, Top2 inhibitors doxorubicin and etoposide, and non–DNA-damaging agent microtubule inhibitor paclitaxel. We observed a higher degree of combination activity, as measured by median synergy scores, with platinum and antimetabolite agent's (range 0.83–4.3), followed by Top1 chemotherapies (0.29–0.38) but little combination activity with Top2 and microtubule agents (–0.03 to 0.14; **Fig. 4A**; Supplementary Fig. S4). Example combination GI_{50} curve shifts for

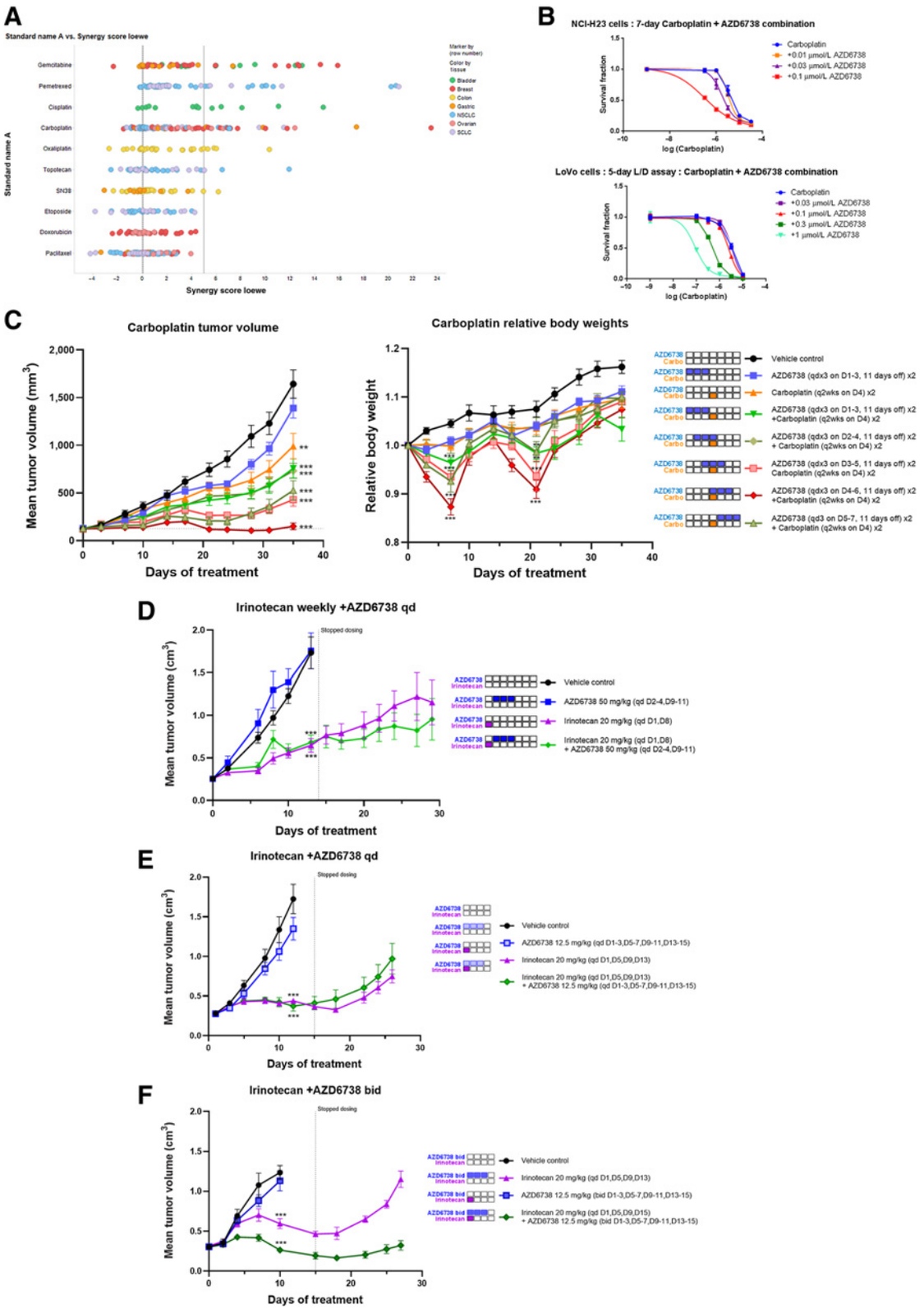
A
Standard name A vs. Synergy score loewe
Standard name A
Gemcitabine
Pemetrexed
Cisplatin
Carboplatin
Oxaliplatin
Topotecan
SN38
Etoposide
Doxorubicin
Paclitaxel
Synergy score loewe
Marker by (row number)
Color by tissue
Bladder
Breast
Colon
Gastric
hSCLC
Ovarian
SCLC
B
NCI-H23 cells : 7-day Carboplatin + AZD6738 combination
Survival fraction
log (Carboplatin)
Carboplatin
+0.01 µmol/L AZD6738
+0.03 µmol/L AZD6738
+0.1 µmol/L AZD6738
LoVo cells : 5-day L/D assay : Carboplatin + AZD6738 combination
Survival fraction
log (Carboplatin)
Carboplatin
+0.03 µmol/L AZD6738
+0.1 µmol/L AZD6738
+0.3 µmol/L AZD6738
+1 µmol/L AZD6738
C
Carboplatin tumor volume
Mean tumor volume (mm3)
Days of treatment
Carboplatin relative body weights
Relative body weight
Days of treatment
Vehicle control
AZD6738 (qdx3 on D1-3, 11 days off) x2
Carboplatin (q2wks on D4) x2
AZD6738 (qdx3 on D1-3, 11 days off) x2 +Carboplatin (q2wks on D4) x2
AZD6738 (qdx3 on D2-4, 11 days off) x2 + Carboplatin (q2wks on D4) x2
AZD6738 (qdx3 on D3-5, 11 days off) x2 Carboplatin (q2wks on D4) x2
AZD6738 (qdx3 on D4-6, 11 days off) x2 +Carboplatin (q2wks on D4) x2
AZD6738 (qd3 on D5-7, 11 days off) x2 + Carboplatin (q2wks on D4) x2
D
Irinotecan weekly +AZD6738 qd
Stopped dosing
Mean tumor volume (cm3)
Days of treatment
Vehicle control
AZD6738 50 mg/kg (qd D2-4,D9-11)
Irinotecan 20 mg/kg (qd D1,D8)
Irinotecan 20 mg/kg (qd D1,D8) + AZD6738 50 mg/kg (qd D2-4,D9-11)
E
Irinotecan +AZD6738 qd
Stopped dosing
Mean tumor volume (cm3)
Days of treatment
Vehicle control
AZD6738 12.5 mg/kg (qd D1-3,D5-7,D9-11,D13-15)
Irinotecan 20 mg/kg (qd D1,D5,D9,D13)
Irinotecan 20 mg/kg (qd D1,D5,D9,D13) + AZD6738 12.5 mg/kg (qd D1-3,D5-7,D9-11,D13-15)
F
Irinotecan +AZD6738 bid
Stopped dosing
Mean tumor volume (cm3)
Days of treatment
Vehicle control
Irinotecan 20 mg/kg (qd D1,D5,D9,D13)
AZD6738 12.5 mg/kg (bid D1-3,D5-7,D9-11,D13-15)
Irinotecan 20 mg/kg (qd D1,D5,D9,D15) + AZD6738 12.5 mg/kg (bid D1-3,D5-7,D9-11,D13-15)

NCI-H23 and LoVo cells are shown in **Fig. 4B**. We compared synergy scores for each combination partner by DDR-proficient or -deficient status (as defined in **Fig. 1** and Supplementary Fig. S1) but observed no significant enrichment for increased synergy in DDR-deficient cell lines (Supplementary Fig. S4B), although the overall dataset is small. These data are broadly consistent with expected mechanism of action with strongest synergies being observed with agents that induce replication stress and across cell lines regardless of DDR status.

Optimal AZD6738 chemotherapy combination antitumor activity *in vivo* is dose and schedule dependent

Next, we wanted to test if *in vitro* combinations translated *in vivo* and to provide insights into optimal dose-schedules, which balances tolerability with efficacy. We established tolerable dose-schedules in mice in combination with carboplatin. We used a clinically relevant dose of carboplatin, 100 mg/kg by intraperitoneal injection in mice and added AZD6738. Compared with monotherapy, we had to dose reduce AZD6738 to 25 mg/kg once daily and employ an intermittent schedule, with a maximum of 3 days consecutive dosing in a 2-weekly cycle (3-days-on/11-days-off) to achieve tolerability. The time off AZD6738 was required for mice to recover and regain body weight before re-dosing (Supplementary Fig. S5). For antitumor studies we used the HBCx-9 TNBC PDX model (BRCA WT, TP53 mutant). Carboplatin and AZD6738 was dosed as either monotherapy or in combination at different sequence-schedules (**Fig. 4C**). We compared AZD6738 dosing before (days 1–3), concurrently (days 2–6), or on the days after (days 5–7) the carboplatin dose (day 4). Clear differences in growth inhibition were observed. Dosing AZD6738 days before carboplatin showed little combination benefit. In contrast, dosing AZD6738 on the days after carboplatin showed significant improvements in combination activity with tumor regressions achievable. Dosing AZD6738 1 day before carboplatin or 1 day after carboplatin gave intermediate activity. When comparing tolerability, the schedules that showed the best antitumor activity also experienced the most, but recoverable, body weight losses.

In combination with the Top1 inhibitor irinotecan we established tolerability with 3 days AZD6738 dosing (days 1–3 and 5–7) in combination with a clinically relevant 20 mg/kg irinotecan dose (twice weekly, days 1 and 5). We found that 25 mg/kg once daily AZD6738 was not well tolerated when dosed concurrently (Supplementary Table S2). However, a dose reduction to 12.5 mg/kg was tolerated. In addition, a higher 50 mg/kg once daily dose administered on 24 hours after irinotecan (AZD6738 days 2–4, irinotecan days 1 and 5) was also tolerated and we tested these regimens for activity in the Colo205 colorectal xenograft model (**Fig. 4D–F**). AZD6738 dosed after irinotecan did not show any combination activity (**Fig. 4D**). Once daily dosing of AZD6738 concurrent with irinotecan did not show any combination activity either (**Fig. 4E**). However, switching to twice daily dosing at 12.5 mg/kg did show significant combination activity and tumor regressions (**Fig. 4F**). These data suggest that sustained ATR inhibition over the first 24 hours is necessary and sufficient to show combination benefit with irinotecan.

AZD6738 combines synergistically with PARP inhibitor olaparib in BRCA1-mutant cells

We investigated the combination with the PARP1/2 inhibitor olaparib, which increases single-stranded DNA breaks and traps PARP1 onto DNA, causing DNA replication stress and activation of ATR–CHK1 signaling axis (Supplementary Fig. S5; refs. 41, 42). The *in vitro* activity of the combination in UWB1.289 BRCA1-mutant cells and compared with its matched pair in which BRCA1 function has been restored through reexpression of WT BRCA1 (34). Olaparib GI_{50} curve shifts in the absence or presence of low 0.1 μmol/L AZD6738 (**Fig. 5A**) showed hypersensitivity of UWB1.289 cells to the combination with 3-log shift in olaparib GI_{50}. In contrast, in the UWB1.289+BRCA1 cell line the combination was far less effective. Notably, AZD6738 monotherapy at 0.1 μmol/L did not show significant growth inhibition, indicating a lower threshold of ATR inhibition is sufficient to potentiate the cell killing effects of olaparib in BRCA-mutant cells.

To further evaluate the mechanisms underlying the combination activity we compared genome instability using metaphase chromosome spread analysis (**Fig. 5B**). Olaparib is expected to generate replication fork associated DNA damage and in combination with ATRi we should increase DSBs formation as well as override the G_2–M cell-cycle checkpoint, leading to progressing into M-phase carrying chromosomal breaks. In line with this, metaphase spread analysis showed the combination significantly increased the mean number of chromosomal aberrations in UWB1.289 cells compared with monotherapies (∼34 aberrations per spread for combination vs. ∼11 or ∼8 for olaparib or AZD6738, respectively). In UWB1.289+BRCA1 cells the mean number of chromosomal aberrations was far lower with only a modest increase observed (∼12 aberrations per spread for combination vs. ∼3 or ∼7 for olaparib or AZD6738, respectively).

AZD6738 in combination with olaparib shows enhanced *in vivo* antitumor activity in BRCA-mutant TNBC PDX models

AZD6738 and olaparib combinations were tested for tolerability and efficacy using different dose-schedules to determine optimal dosing regimens. We found that the olaparib monotherapy dose of 100 mg/kg once daily was not well tolerated when combined concurrently with AZD6738 at >25 mg/kg doses at any schedule tested. However, dose reduction to 12.5 mg/kg twice daily AZD6738 in up to 2 week 'blocks' (14-days-on/14-days-off) was tolerated. We explored reducing the dose of olaparib to 50 mg/kg once daily and by using an intermittent 3-days-on/4-days-off or 5-days-on/2-days-off weekly schedule, which was also tolerated. With these regimens we evaluated

Figure 4.

AZD6738 in combination with DNA-damaging chemotherapy. **A,** Dot plots of *in vitro* cell line screen with AZD6738 in combination with the indicated DNA damaging chemotherapies. Combination synergy scores (Loewe) were calculated for each cell line and combination where values greater than 5 are considered overall synergistic and values between 1 and 5 overall additive. Each cell line is labeled by a dot. **B,** Representative example of carboplatin GI_{50} curve shifts by fixed concentration of AZD6738 in NCI-H23 and LoVo cells *in vitro*. Efficacy *in vivo* for carboplatin in combination with AZD6738 in human breast cancer PDX model HBCx-9 at the indicated doses and schedules. **C,** Antitumor combination efficacy and relative body weight losses are dependent on sequence of AZD6738 administration relative to carboplatin. Dosing on days after carboplatin is required for efficacy. Mean tumor volume ± SEM is shown. Body weight loss for combination with carboplatin is also dependent on sequence of administration, with animals with dosing on days after carboplatin experiencing more, but recoverable body weight losses. Mean body weights at time of treatment relative to starting weights are shown. Statistical differences were assessed on day 7 and day 21 nadir's only. **D–F,** Efficacy *in vivo* for irinotecan in combination with AZD6738 in human colorectal cell line xenograft Colo205 using AZD6738 (**D**) was dosed after irinotecan, low-dose AZD6738 was dosed once daily concurrently with irinotecan (**E**), or low-dose AZD6738 (**F**) was dosed twice daily concurrently after twice weekly irinotecan. Mean tumor volume ± SEM is shown. **, $P \le 0.01$; ***, $P \le 0.001$.

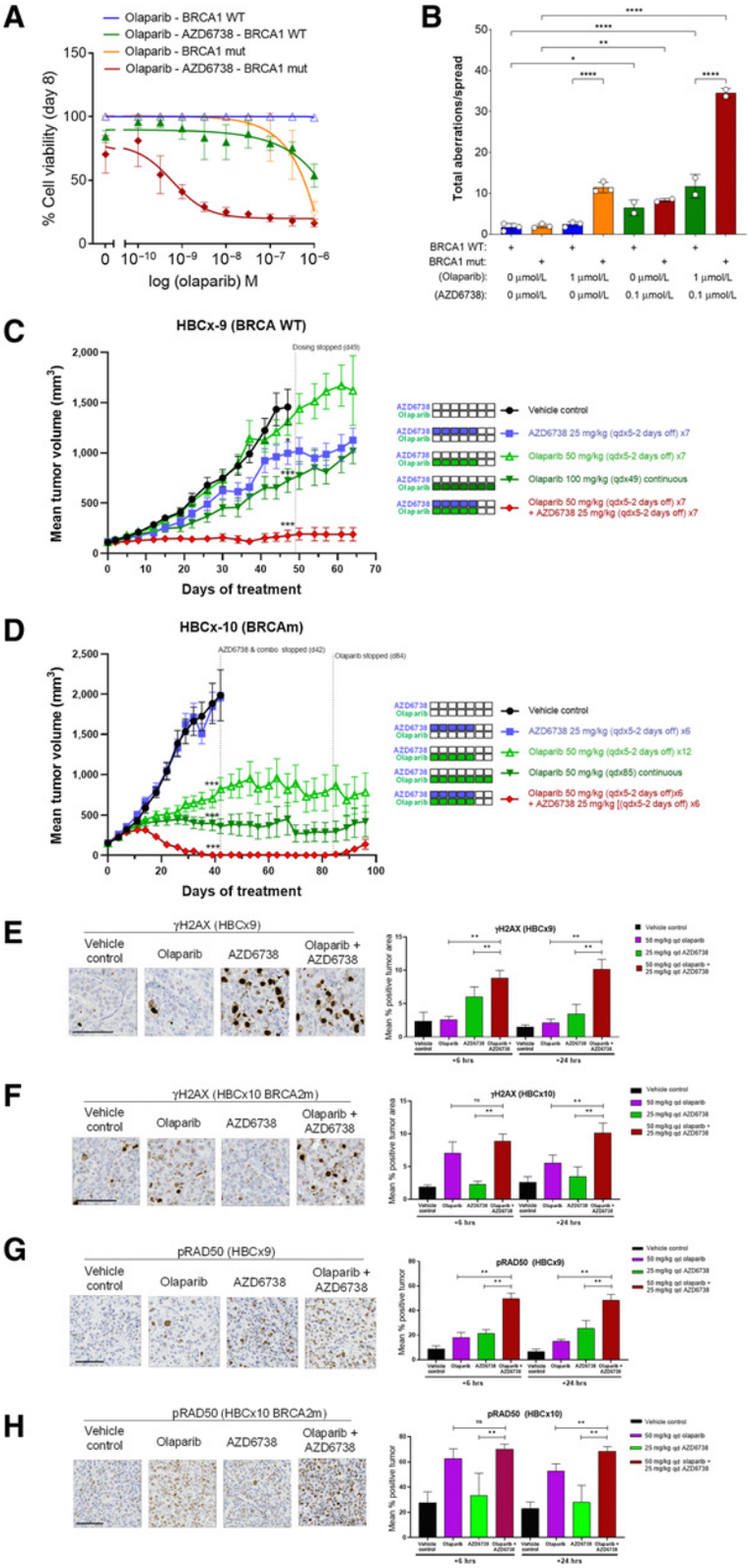

Figure 5.

AZD6738 combination with the PARP inhibitor olaparib. **A,** AZD6738 potentiates the activity of olaparib and shows synergistic growth inhibition of BRCA1-mutant (Δ11q) UWB1.289 cells preferentially over UWB1.289+BRCA1–complemented cells. Representative growth inhibition plots are shown. **B,** Metaphase spreads for AZD6738 and olaparib combination shows a synergistic increase in chromosomal aberrations in UWB1.289 compared with UWB1.289+BRCA1–complemented cells. **C** and **D,** *In vivo* efficacy of olaparib in combination with AZD6738 in TNBC PDX models using 50 mg/kg once daily olaparib plus 25 mg/kg AZD6738 on 5 days-on/2 days-off weekly schedule (×6) in HBCx-9 BRCA WT (**C**) or HBCx-10 BRCA2-mutant model (**D**). Mean tumor volume ± SEM is shown. Olaparib and AZD6738 combination pharmacodynamics by IHC in HBCx-9 WT and HBCx-10 BRCA2-mutant models. **E–H,** Representative images at 6 hours post last dose (left) and quantification (% positive cells; right) for γH2AX in HBCx-9 (**E**) or HBCx-10 (**F**), and pRAD50 pSer635 in HBCx-9 (**G**) or HBCx-10 (**H**) models. Scale bars, 100 μm. *, $P \le 0.05$; **, $P \le 0.01$; ***, $P \le 0.001$; ****, $P \le 0.0001$.

combination activity in both HBCx-10 BRCA2-mutant and HBCx-9 BRCA WT TNBC PDX models (36). In the HBCx-10 model (**Fig. 5C**) we observed significant efficacy with 50 mg/kg once daily olaparib plus 25 mg/kg once daily AZD6738 5-days-on/2-days-off weekly schedules with complete responses by ∼35 days and with durable tumor suppression lasting a further ∼40 days after cessation of dosing before regrowth. Equivalent monotherapies showed stasis for olaparib while AZD6738 was inactive. In comparison the HBCx-9 model (**Fig. 5D**), combination activity was modest (tumor stasis) but was still significantly improved compared with equivalent monotherapies. The differential response to the combination between BRCA-mutant and WT *in vivo* models is consistent the differential activity observed *in vitro*.

We then assessed how γH2AX and pRAD50 biomarkers were modulated by the combination. 50 mg/kg once daily olaparib and 25 mg/kg once daily AZD6738 were dosed as monotherapy or in combination for 7 consecutive days and tumors harvested at 6 hours and 24 hours after the 7th daily dose. In HBCx-9 model olaparib monotherapy did not induce γH2AX (**Fig. 5E**) while AZD6738 monotherapy showed a time-dependent increase that peaked at 6 hours but dropped to baseline by 24 hours. The combination group showed further increases and was sustained over 24 hours. This pattern of induction is generally consistent with the relative antitumor activities in this model (**Fig. 5C**), with stronger induction of the biomarkers associated with greater antitumor response. The pattern of γH2AX induction in the HBCx-10 BRCA-mutant model (**Fig. 5F**) also followed the antitumor response (**Fig. 5D**), with olaparib monotherapy showing robust γH2AX induction while AZD6738 showed no increase and the combination showed further increases, which were sustained over 24 hours. pRAD50 induction (**Fig. 5G** and **H**) showed a similar pattern but the magnitude was larger than γH2AX. The lack of induction of γH2AX by AZD6738 alone in the HBCx-10 model in unclear.

AZD6738 and olaparib combination antitumor activity *in vivo* is dependent on dose and schedule

We further explored the AZD6738 and olaparib combination determine optimal dose-schedule-efficacy relationship. In the HBCx-10 BRCAm PDX model, which was highly responsive to the combination using a 5-days-on/2-days-off schedule, we wanted to determine the minimum dose-schedules required for tumor regression. We compared a shorter 3-days-on/4-days-off AZD6738 schedule in combination with 5-days-on/2-days-off olaparib or continuous daily olaparib (**Fig. 6A**). Using 3 days of AZD6738 we still observed significant combination activity and tumor regressions, however the time to tumor stasis was longer compared with the longer 5-day schedule (**Fig. 5C**), indicating the additional 2 days AZD6738 dosing per week conferred an improved responses. In contrast, when olaparib was increased from 5-days-on/2-days-off to a continuous daily schedule, we observed no difference in %TGI, indicating that additional days on low-dose olaparib in the absence of AZD6738 adds little benefit. We then assessed whether increasing the doses of olaparib from 50 mg/kg to 100 mg/kg and AZD6738 from 25 mg/kg to 50 mg/kg on the short 3-days-on/4-days-off schedule would improve efficacy. To achieve tolerability we had to dose compounds 8 hours apart (AZD6738 after olaparib), but even so we were able to observe complete regressions (**Fig. 6B** comparable to the longer 5-days-on/2-day-off schedule **Fig. 5C**). These data indicate that combination efficacy is also affected by dose and increasing olaparib and AZD6738 (to levels equivalent to monotherapy) is able to compensate for the short 3 days dosing in BRCA-mutant model.

In the less responsive HBCx-9 PDX model we assessed whether we could improve efficacy by altering dose-schedules. We increased dose intensity by employing a low 12.5 mg/kg twice daily AZD6738 dose but on a 14-days-on "block" in combination with continuous olaparib (**Fig. 6C**). We observed significant antitumor activity with complete regressions compared with only tumor growth delay by the monotherapies. This combination schedule showed a marked improvement in efficacy over the 5-days-on/2-days-off weekly schedule (**Fig. 5D**). These data demonstrate that in combination with olaparib increasing the number of AZD6738 doses is able to drive significant improvements in efficacy, even in a BRCA WT setting.

Overall these data confirm BRCA-mutant models are more sensitive to the combination compared with BRCA WT models, requiring lower doses and shorter durations achieve regressions. Moreover, we observe that AZD6738 is the main determinant of activity for the combination. A dose-schedule relationship was established whereby higher doses/shorter durations can give equivalent efficacy to lower doses/longer durations providing flexibility of dosing in the clinic.

Discussion

Here we report on the biological activity of AZD6738 (ceralasertib), an orally bioavailable inhibitor of ATR currently being investigated in early clinical trials (4, 5). AZD6738 modulates ATR/ATM/DNA-PK signaling and homologous recombination-mediated repair, while selectively inhibiting the growth of subsets of cancer models. AZD6738 demonstrated significant antitumor growth control as monotherapy, whereas tumor regressions can be achieved in combination with carboplatin, irinotecan or olaparib. Moreover, we provide additional insights into the optimal dose-schedules for tolerability and efficacy each of the combinations.

AZD6738 monotherapy activity across *in vitro* cell line panels show that not all cells are sensitive ATR inhibition, which was a safety concern for targeting ATR, which is thought to be an essential gene for cell survival (3). In fact, we observed a wide range of responses with GI_{50}'s from 10 nmol/L to >30 μmol/L (inactive). The selective sensitivity of subsets of cell lines potentially reveals patient selection opportunities if they can be associated with specific molecular aberrations. While we were unable to identify a single unifying gene aberration that explained sensitivity, we did find significant enrichments (but not limited to) with CCNE1 copy number, ARID1A, ATRX, and SETD2 mutations as well ATM loss-of-function. Reassuringly, the links between ATM, ARID1A, SETD2, and CCNE1 with ATRi sensitivity and/or replication stress have been previously described (3, 8–11, 18, 43–45), although we did not observe any association with BRCA1/2 mutations. AZD6738 showed dose-dependent induction of DSB signaling (pRAD50, pKAP1, pDNA-PK) and DNA damage markers (γH2AX, pRPA) *in vitro* and *in vivo*. Our findings are broadly consistent with data recently reported for a different ATRi BAY-1895344 in preclinical models (Supplementary Fig. S3B; ref. 46) and in phase I clinical study (47), suggesting these biomarker inductions are 'on-target' common features of single agent ATR inhibition. These observations suggest a codependency between ATR inhibition and induction DSB pathways such as through ATM. Analysis of cell line panels for sensitivity and any ATM mutation did not reveal a significant correlation, but only when functional assessments (ATM-deficient) were performed was the association revealed. This supports the notion that some ATM mutations, e.g., missense or monoallelic, are insufficient to confer ATRi sensitivity. While out-of-scope for the work described here, it

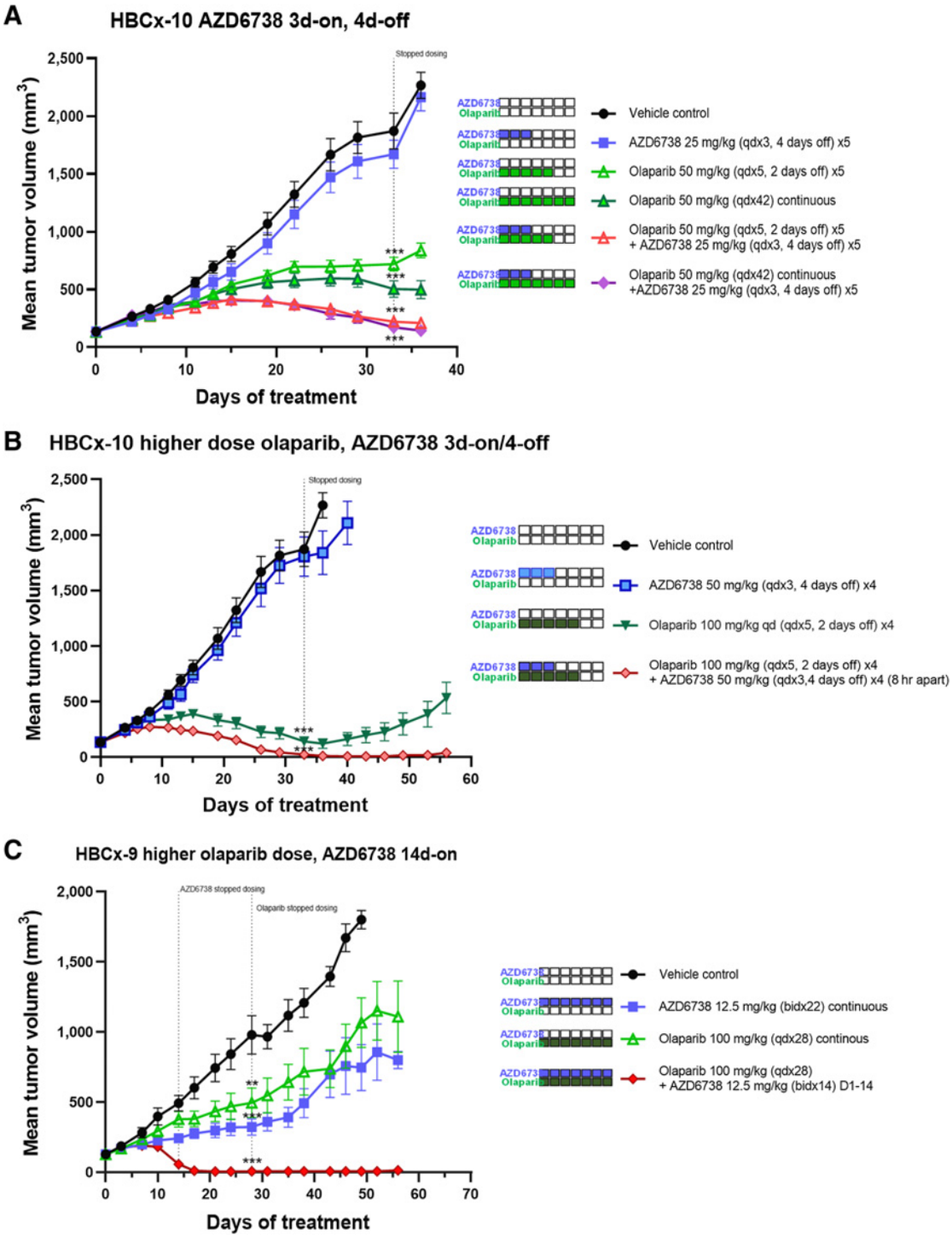

Figure 6.

AZD6738 combination with the PARP inhibitor olaparib efficacy using alternative dose schedules. **A,** HBCx-10 BRCA-mutant TNBC PDX efficacy when AZD6738 is dosed 3 days-on/4 days-off in combination with low-dose olaparib either on a 5 days-on/2 days-off or continuous daily dosing backbone. **B,** HBCx-10 BRCA-mutant TNBC PDX when AZD6738 is dosed on 3 days-on/4 days-off in combination with high-dose olaparib on a 5 days-on/2 days-off schedule. **C,** HBCx-9 BRCA WT TNBC PDX model efficacy when low-dose AZD6738 is dosed twice daily in combination with high-dose olaparib on continuous daily schedule. Mean tumor volume ± SEM is shown. **, $P \leq 0.01$; ***, $P \leq 0.001$.

could have important implications for selecting patients and suggest care should be taken by only considering biallelic deleterious mutations and/or ATM-null expression.

While we observe significant *in vivo* antitumor efficacy with AZD6738 monotherapy the best responses are typically tumor control/stasis. In order to improve efficacy, ATRis could be used in combination with DNA damaging agents such as carboplatin or irinotecan. When used in these combinations lower doses and durations of AZD6738 could be used that achieves significantly better efficacy than monotherapies. However, a major challenge to implement this successfully will be normal tissue toxicity. One strategy to widen the therapeutic margin is identifying tumor-specific molecular vulnerabilities that show enhanced sensitivities to combinations such as ATM loss with cisplatin (25) or BRCA/ATM with olaparib (29, 30). Another, complementary approach described here is to optimize the dose schedules and determine the minimum target coverages required for efficacy while managing tolerability. Targeting the right tumor genetics along with optimized dose–sequence schedules will likely be key to clinical success for ATRi.

We find that AZD6738 is generally tolerated when dosed for ∼3 days in combination with chemotherapy before a dosing holiday needs to be introduced. The recovery time varied between agents used and efficacy was highly dependent on the AZD6738 schedule. The most efficacious schedule was to dose AZD6738 concurrently with chemotherapy. For carboplatin it was also important to continue AZD6738 dosing on the days after carboplatin to show tumor regressions. In contrast, for irinotecan concurrent dosing over day 1 was necessary and sufficient for tumor regressions. Dosing AZD6738 before chemotherapy did not confer benefit and confirms ATR activity is only relevant following DNA damage. Together these data highlight the importance of studies assessing the dose-sequence for each individual chemotherapy partner, which may inform combination strategies in the clinic.

Olaparib combinations also showed dose-schedule dependency but was overall better tolerated allowing greater dose intensities and responses. BRCA-mutant TNBC PDX models also conferred enhanced sensitivity toward the combination, which is consistent with previous reports in ovarian cancer models (29). In our studies we compared different dose-schedules in both BRCA-mutant and WT TNBC PDX models. Duration of dosing was a major determinant of efficacy and by increasing AZD6738 doses from 3 to ≥5 days improved responses. This was particularly apparent in BRCA WT HBCx-9 model where only longer durations of AZD6738 dosing achieved tumor regressions. The ability of AZD6738 to inhibit BIR and HRR pathways is intriguing and, for BIR, which primarily repairs collapsed replication forks, could be expected but as far as we are aware this is the first time this has been directly reported. Whether the level of HR suppression we observed is sufficient to induce a "BRCAness" phenotype and contributes towards sensitivity to olaparib combination remains to be elucidated.

Here we demonstrate the preclinical activity of AZD6738 as monotherapy and in combination with chemotherapy and olaparib while providing insights into the dose-scheduling requirements. A large number of clinical trials with AZD6738 and other ATRis are currently underway.

Authors' Disclosures

Y. Wallez reports being an employee of AstraZeneca. P.W.G. Wijnhoven reports being an AstraZeneca stakeholder. G.N. Jones reports personal fees from AstraZeneca during the conduct of the study and personal fees from AstraZeneca outside the submitted work. M.J. O'Connor reports being a full-time employee and shareholder at AstraZeneca. A. Lau reports other support from AstraZeneca outside the submitted work and being an employee and shareholder in AstraZeneca. No disclosures were reported by the other authors.

Authors' Contributions

Z. Wilson: Data curation, formal analysis, supervision, validation, investigation, visualization, methodology, project administration, writing–review and editing. **R. Odedra:** Formal analysis, supervision, validation, investigation, visualization, methodology. **Y. Wallez:** Formal analysis, investigation, visualization, methodology, writing–review and editing. **P.W.G. Wijnhoven:** Formal analysis, investigation, visualization, methodology, writing–review and editing. **A.M. Hughes:** Formal analysis, investigation, visualization, writing–review and editing. **J. Gerrard:** Formal analysis, investigation, visualization. **G.N. Jones:** Formal analysis, investigation, visualization, writing–review and editing. **H. Bargh-Dawson:** Formal analysis, investigation, visualization, methodology. **E. Brown:** Investigation, methodology. **L.A. Young:** Formal analysis, investigation, visualization. **M.J. O'Connor:** Supervision, validation, writing–review and editing. **A. Lau:** Conceptualization, formal analysis, supervision, validation, visualization, writing–original draft, project administration, writing–review and editing.

Acknowledgments

The authors acknowledge Aaron Smith and Graeme Scarfe for DMPK and physicochemical property characterization; James Yates for pharmacokinetic modeling; Benjamin Taylor and Jenni Nikkila for plasmid generation for the BIR and TLR reporter assays. They thank the AstraZeneca Laboratory Animal Sciences and Oncology *in vivo* teams for their support and expert technical assistance. The authors thank XenTech SAS for their assistance with PDX studies. They thank Emma Dean and members of core ATR project team for help with preparing the manuscript. Special mention should be given to Xavier Jacq, Aaron Cranston, Lisa Smith, and Sylvie Guichard for their early work on ATRi development and all past and present members of the ATRi project.

The costs of publication of this article were defrayed in part by the payment of page charges. This article must therefore be hereby marked *advertisement* in accordance with 18 U.S.C. Section 1734 solely to indicate this fact.

Received September 6, 2021; revised November 10, 2021; accepted January 19, 2022; published first January 25, 2022.

References

1. Cimprich KA, Cortez D. ATR: an essential regulator of genome integrity. Nat Rev Mol Cell Biol 2008;9:616–27.
2. Forment JV, O'Connor MJ. Targeting the replication stress response in cancer. Pharmacol Ther 2018;188:155–67.
3. Foote KM, Lau A, Nissink JW. Drugging ATR: progress in the development of specific inhibitors for the treatment of cancer. Future Med Chem 2015;7:873–91.
4. Sundar R, Brown J, Ingles Russo A, Yap TA. Targeting ATR in cancer medicine. Curr Probl Cancer 2017;41:302–15.
5. Barnieh FM, Loadman PM, Falconer RA. Progress towards a clinically successful ATR inhibitor for cancer therapy. Curr Res Pharmacol Drug Discov 2021;2:100017.
6. Foote KM, Nissink JWM, McGuire T, Turner P, Guichard S, Yates JWT, et al. Discovery and characterization of AZD6738, a potent inhibitor of ataxia telangiectasia mutated and Rad3-related (ATR) kinase with application as an anticancer agent. J Med Chem 2018;61:9889–907.
7. Foote KM, Blades K, Cronin A, Fillery S, Guichard SS, Hassall L, et al. Discovery of 4-{4-[(3R)-3-Methylmorpholin-4-yl]-6-[1-(methylsulfonyl)cyclopropyl]pyrimidin-2-yl}-1H-indole (AZ20): a potent and selective inhibitor of ATR protein kinase with monotherapy *in vivo* antitumor activity. J Med Chem 2013;56:2125–38.
8. Reaper PM, Griffiths MR, Long JM, Charrier JD, Maccormick S, Charlton PA, et al. Selective killing of ATM- or p53-deficient cancer cells through inhibition of ATR. Nat Chem Biol 2011;7:428–30.
9. Kwok M, Davies N, Agathanggelou A, Smith E, Oldreive C, Petermann E, et al. ATR inhibition induces synthetic lethality and overcomes chemoresistance in TP53- or ATM-defective chronic lymphocytic leukemia cells. Blood 2016;127:582–95.

10. Min A, Im SA, Jang H, Kim S, Lee M, Kim DK, et al. AZD6738, a novel oral inhibitor of ATR, induces synthetic lethality with ATM deficiency in gastric cancer cells. Mol Cancer Ther 2017;16:566–77.
11. Schmitt A, Knittel G, Welcker D, Yang TP, George J, Nowak M, et al. ATM deficiency is associated with sensitivity to PARP1- and ATR inhibitors in lung adenocarcinoma. Cancer Res 2017;77:3040–56.
12. Middleton FK, Patterson MJ, Elstob CJ, Fordham S, Herriott A, Wade MA, et al. Common cancer-associated imbalances in the DNA damage response confer sensitivity to single agent ATR inhibition. Oncotarget 2015;6:32396–409.
13. Mohni KN, Kavanaugh GM, Cortez D. ATR pathway inhibition is synthetically lethal in cancer cells with ERCC1 deficiency. Cancer Res 2014;74:2835–45.
14. Sultana R, Abdel-Fatah T, Perry C, Moseley P, Albarakti N, Mohan V, et al. Ataxia telangiectasia mutated and Rad3-related (ATR) protein kinase inhibition is synthetically lethal in XRCC1 deficient ovarian cancer cells. PLoS One 2013;8:e57098.
15. Nikkila J, Kumar R, Campbell J, Brandsma I, Pemberton HN, Wallberg F, et al. Elevated APOBEC3B expression drives a kataegic-like mutation signature and replication stress-related therapeutic vulnerabilities in p53-defective cells. Br J Cancer 2017;117:113–23.
16. Buisson R, Lawrence MS, Benes CH, Zou L. APOBEC3A and APOBEC3B activities render cancer cells susceptible to ATR inhibition. Cancer Res 2017;77:4567–78.
17. Henssen AG, Reed C, Jiang E, Garcia HD, von Stebut J, MacArthur IC, et al. Therapeutic targeting of PGBD5-induced DNA repair dependency in pediatric solid tumors. Sci Transl Med 2017;9:eaam9078.
18. Williamson CT, Miller R, Pemberton HN, Jones SE, Campbell J, Konde A, et al. ATR inhibitors as a synthetic lethal therapy for tumors deficient in ARID1A. Nat Commun 2016;7:13837.
19. Kurashima K, Kashiwagi H, Shimomura I, Suzuki A, Takeshita F, Mazevet M, et al. SMARCA4 deficiency-associated heterochromatin induces intrinsic DNA replication stress and susceptibility to ATR inhibition in lung adenocarcinoma. NAR Cancer 2020;2:zcaa005.
20. Nguyen HD, Leong WY, Li W, Reddy PNG, Sullivan JD, Walter MJ, et al. Spliceosome mutations induce R loop–associated sensitivity to ATR inhibition in myelodysplastic syndrome. Cancer Res 2018;78:5363–74.
21. Wang C, Wang G, Feng X, Shepherd P, Zhang J, Tang M, et al. Genome-wide CRISPR screens reveal synthetic lethality of RNASEH2 deficiency and ATR inhibition. Oncogene 2019;38:2451–63.
22. Dunne V, Ghita M, Small DM, Coffey CBM, Weldon S, Taggart CC, et al. Inhibition of ataxia telangiectasia related-3 (ATR) improves therapeutic index in preclinical models of non–small cell lung cancer (NSCLC) radiotherapy. Radiother Oncol 2017;124:475–81.
23. Dillon MT, Bergerhoff KF, Pedersen M, Whittock H, Crespo-Rodriguez E, Patin EC, et al. ATR inhibition potentiates the radiation-induced inflammatory tumor microenvironment. Clin Cancer Res 2019;25:3392–403.
24. Vendetti FP, Karukonda P, Clump DA, Teo T, Lalonde R, Nugent K, et al. ATR kinase inhibitor AZD6738 potentiates $CD8^+$ T cell–dependent antitumor activity following radiation. J Clin Invest 2018;128:3926–40.
25. Vendetti FP, Lau A, Schamus S, Conrads TP, O'Connor MJ, Bakkenist CJ. The orally active and bioavailable ATR kinase inhibitor AZD6738 potentiates the antitumor effects of cisplatin to resolve ATM-deficient non–small cell lung cancer *in vivo*. Oncotarget 2015;6:44289–305.
26. Josse R, Martin SE, Guha R, Ormanoglu P, Pfister TD, Reaper PM, et al. ATR inhibitors VE-821 and VX-970 sensitize cancer cells to topoisomerase i inhibitors by disabling DNA replication initiation and fork elongation responses. Cancer Res 2014;74:6968–79.
27. Young LA, O'Connor LO, de Renty C, Veldman-Jones MH, Dorval T, Wilson Z, et al. Differential activity of ATR and WEE1 inhibitors in a highly sensitive subpopulation of DLBCL linked to replication stress. Cancer Res 2019;79:3762–75.
28. Wallez Y, Dunlop CR, Johnson TI, Koh SB, Fornari C, Yates JWT, et al. The ATR inhibitor AZD6738 synergizes with gemcitabine *in vitro* and *in vivo* to induce pancreatic ductal adenocarcinoma regression. Mol Cancer Ther 2018;17:1670–82.
29. Kim H, George E, Ragland R, Rafial S, Zhang R, Krepler C, et al. Targeting the ATR/CHK1 axis with PARP inhibition results in tumor regression in BRCA-mutant ovarian cancer models. Clin Cancer Res 2017;23:3097–108.
30. Lloyd RL, Wijnhoven PWG, Ramos-Montoya A, Wilson Z, Illuzzi G, Falenta K, et al. Combined PARP and ATR inhibition potentiates genome instability and cell death in ATM-deficient cancer cells. Oncogene 2020;39:4869–83.
31. Crafter C, Vincent JP, Tang E, Dudley P, James NH, Klinowska T, et al. Combining AZD8931, a novel EGFR/HER2/HER3 signaling inhibitor, with AZD5363 limits AKT inhibitor induced feedback and enhances antitumor efficacy in HER2-amplified breast cancer models. Int J Oncol 2015;47:446–54.
32. Costantino L, Sotiriou SK, Rantala JK, Magin S, Mladenov E, Helleday T, et al. Break-induced replication repair of damaged forks induces genomic duplications in human cells. Science 2014;343:88–91.
33. Certo MT, Ryu BY, Annis JE, Garibov M, Jarjour J, Rawlings DJ, et al. Tracking genome engineering outcome at individual DNA breakpoints. Nat Methods 2011;8:671–6.
34. DelloRusso C, Welcsh PL, Wang W, Garcia RL, King MC, Swisher EM. Functional characterization of a novel BRCA1-null ovarian cancer cell line in response to ionizing radiation. Mol Cancer Res 2007;5:35–45.
35. Kilkenny C, Browne WJ, Cuthill IC, Emerson M, Altman DG. Improving bioscience research reporting: the ARRIVE guidelines for reporting animal research. PLoS Biol 2010;8:e1000412.
36. Castroviejo-Bermejo M, Cruz C, Llop-Guevara A, Gutierrez-Enriquez S, Ducy M, Ibrahim YH, et al. A RAD51 assay feasible in routine tumor samples calls PARP inhibitor response beyond BRCA mutation. EMBO Mol Med 2018;10:e9172.
37. Riches LC, Trinidad AG, Hughes G, Jones GN, Hughes AM, Thomason AG, et al. Pharmacology of the ATM inhibitor AZD0156: potentiation of irradiation and olaparib responses preclinically. Mol Cancer Ther 2020;19:13–25.
38. Jones GN, Rooney C, Griffin N, Roudier M, Young LA, Garcia-Trinidad A, et al. pRAD50: a novel and clinically applicable pharmacodynamic biomarker of both ATM and ATR inhibition identified using mass spectrometry and immunohistochemistry. Br J Cancer 2018;119:1233–43.
39. Krebs MG, Lopez J, El-Khoueiry A, Bang Y-J, Postel-Vinay S, Abida W, et al. Abstract CT026: Phase I study of AZD6738, an inhibitor of ataxia telangiectasia Rad3-related (ATR), in combination with olaparib or durvalumab in patients (pts) with advanced solid cancers. Cancer Res 2018;78:CT026.
40. Berges A, Cheung SYA, Pierce AJ, Dean E, Felicetti B, Standifer N, et al. Abstract CT118: PK-biomarker-safety modelling aids choice of recommended phase II dose and schedule for AZD6738 (ATR inhibitor). Cancer Res 2018;78:CT118.
41. Parsels LA, Karnak D, Parsels JD, Zhang Q, Velez-Padilla J, Reichert ZR, et al. PARP1 trapping and DNA replication stress enhance radiosensitization with combined WEE1 and PARP inhibitors. Mol Cancer Res 2018;16:222–32.
42. Murai J, Huang SY, Das BB, Renaud A, Zhang Y, Doroshow JH, et al. Trapping of PARP1 and PARP2 by clinical PARP inhibitors. Cancer Res 2012;72:5588–99.
43. Pfister SX, Markkanen E, Jiang Y, Sarkar S, Woodcock M, Orlando G, et al. Inhibiting WEE1 selectively kills histone H3K36me3-deficient cancers by dNTP starvation. Cancer Cell 2015;28:557–68.
44. Jones RM, Mortusewicz O, Afzal I, Lorvellec M, Garcia P, Helleday T, et al. Increased replication initiation and conflicts with transcription underlie Cyclin E-induced replication stress. Oncogene 2013;32:3744–53.
45. Llobet GS, van der Vegt B, Jongeneel E, Bense RD, Zwager MC, Schroder CP, et al. Cyclin E expression is associated with high levels of replication stress in triple-negative breast cancer. NPJ Breast Cancer 2020;6:40.
46. Wengner AM, Siemeister G, Lucking U, Lefranc J, Wortmann L, Lienau P, et al. The novel ATR inhibitor BAY 1895344 is efficacious as monotherapy and combined with DNA damage-inducing or repair-compromising therapies in preclinical cancer models. Mol Cancer Ther 2020;19:26–38.
47. Yap TA, Tan DSP, Terbuch A, Caldwell R, Guo C, Goh BC, et al. First-in-human trial of the oral ataxia telangiectasia and Rad3-related (ATR) inhibitor BAY 1895344 in patients with advanced solid tumors. Cancer Discov 2021;11:80–91.